



## Recent experimental data may point to a greater role for osmotic pressures in the subsurface

C. E. Neuzil<sup>1</sup> and A. M. Provost<sup>1</sup>

Received 17 August 2007; revised 26 November 2008; accepted 24 December 2008; published 12 March 2009.

[1] Uncertainty about the origin of anomalous fluid pressures in certain geologic settings has caused researchers to take a second look at osmosis, or flow driven by chemical potential differences, as a pressure-generating process in the subsurface. Interest in geological osmosis has also increased because of an in situ experiment by Neuzil (2000) suggesting that Pierre Shale could generate large osmotic pressures when highly compacted. In the last few years, additional laboratory and in situ experiments have greatly increased the number of data on osmotic properties of argillaceous formations, but they have not been systematically examined. In this paper we compile these data and explore their implications for osmotic pressure generation in subsurface systems. Rather than base our analysis on osmotic efficiencies, which depend strongly on concentration, we calculated values of a quantity we term osmotic specific surface area ( $A_{so}$ ) that, in principle, is a property of the porous medium only. The  $A_{so}$  values are consistent with a surprisingly broad spectrum of osmotic behavior in argillaceous formations, and all the formations tested exhibited at least a modest ability to generate osmotic pressure. It appears possible that under appropriate conditions some formations can be highly effective osmotic membranes able to generate osmotic pressures exceeding 30 MPa (3 km of head) at porosities as high as  $\sim 0.1$  and pressures exceeding 10 MPa at porosities as high as  $\sim 0.2$ . These findings are difficult to reconcile with the lack of compelling field evidence for osmotic pressures, and we propose three explanations for the disparity: (1) Our analysis is flawed and argillaceous formations are less effective osmotic membranes than it suggests; (2) the necessary subsurface conditions, significant salinity differences within intact argillaceous formations, are rare; or (3) osmotic pressures are unlikely to be detected and are not recognized when encountered. The last possibility, that osmotic pressures routinely escape detection or are attributed to other mechanisms, has important implications for understanding subsurface flow regimes.

**Citation:** Neuzil, C. E., and A. M. Provost (2009), Recent experimental data may point to a greater role for osmotic pressures in the subsurface, *Water Resour. Res.*, 45, W03410, doi:10.1029/2007WR006450.

### 1. Introduction

[2] Anomalous fluid pressures offer important clues to the nature of subsurface environments. Most appear to result from physical forcing, or perturbation, by dynamic geologic processes, but some occur in stable settings where such processes seem absent [e.g., Bredehoeft *et al.*, 1994; Lee and Deming, 2002]. It has been suggested that osmosis, or fluid flow caused by differences in chemical potential, can explain some of these anomalies [e.g., Marine and Fritz, 1981; Gonçalvès *et al.*, 2004; Gueutin *et al.*, 2007]. This idea remains controversial, in part because of a near absence of data on osmotic properties of geologic formations (as distinct from refined or otherwise processed clays). Indeed, this deficiency prompted one of us to conduct an in situ osmosis test in the Pierre Shale, a moderately compacted Cretaceous claystone with an unusually high clay content

[Neuzil, 2000]. Analysis suggested that if further compacted, the Pierre Shale could generate sizable osmotic pressures. However, it remains unclear how representative that finding is.

[3] Since the Pierre Shale study, the osmotic behavior of a number of other formations has been observed in both laboratory and in situ tests and reported in the literature. Obtained for a variety of purposes, these data have never been considered in toto, perhaps in part because of the difficulty of comparing the experiments. In this paper we propose that a quantity we have termed osmotic specific surface area ( $A_{so}$ ) can be used to compare the results of different experiments and to characterize a formation's ability to generate osmotic pressures. Values of  $A_{so}$  computed from the new data reinforce the notion that osmosis should be a significant pressure-generating mechanism in the subsurface. Indeed, we were surprised to find that about half the argillaceous formations tested appear to be better osmotic membranes than the Pierre Shale, some significantly so. In this paper we present a compilation of these data, describe calculations of  $A_{so}$  values and the osmotic pressures they

<sup>1</sup>U.S. Geological Survey, Reston, Virginia, USA.

imply can be generated, and critically consider the credibility of osmosis as a subsurface pressure-generating mechanism.

## 2. Osmosis and Osmotic Pressure

[4] Osmosis is fluid flow through a semipermeable medium, or membrane, driven by gradients in chemical potential that exist in the presence of spatial variations in solute concentration. Semipermeable membranes retard the flow of solute relative to the solvent, which is water in this context. Clays are known to exhibit semipermeability, and pore fluid flow in them appears to be described by a generalized version of Darcy's law which can be written as [e.g., *Bresler*, 1973]

$$\mathbf{q} = -\frac{k}{\mu}(\nabla p + \rho g \nabla z) + \sigma \frac{k}{\mu} \nabla \pi. \quad (1)$$

Here the vector  $\mathbf{q}$  is the Darcy flux of pore fluid [ $\text{L}^3 \text{L}^{-2} \text{T}^{-1}$ ],  $k$  is permeability [ $\text{L}^2$ ],  $\mu$  is dynamic viscosity [ $\text{M L}^{-1} \text{T}^{-1}$ ],  $p$  is pore fluid pressure [ $\text{M L}^{-1} \text{T}^{-2}$ ],  $\rho$  is pore fluid density [ $\text{M L}^{-3}$ ],  $g$  is gravitational acceleration [ $\text{L T}^{-2}$ ],  $z$  is elevation [ $\text{L}$ ],  $\sigma$  is osmotic efficiency [dimensionless], and  $\pi$  is a quantity often called "osmotic pressure" [ $\text{M L}^{-1} \text{T}^{-2}$ ]. The osmotic efficiency  $\sigma$  is a measure of a membrane's ability to retard the transport of solute relative to water; it takes values from 0, indicating no retardation and no osmotic properties, to 1, indicating a perfect osmotic membrane that allows no solute transport.

[5] Although  $\pi$  has the same dimensions as pressure, it is not a pressure per se, but a measure of the decrease in chemical potential of water due to the presence of solute. It is defined as [e.g., *Robinson and Stokes*, 2002]

$$\pi = -\left(\frac{RT}{V_w}\right) \ln(a_w), \quad (2)$$

where  $R$  is the gas constant [ $\text{M L}^2 \text{T}^{-2} \Theta^{-1} \text{mol}^{-1}$ ],  $T$  is temperature [ $\Theta$ ],  $V_w$  is the molar volume of water [ $\text{L}^3 \text{mol}^{-1}$ ], and  $a_w$  is the water activity [dimensionless]. The quantity  $\pi$  is equivalent to the maximum fluid pressure difference a perfect membrane ( $\sigma = 1$ ) can generate when it separates pore fluid with water activity  $a_w$  from pure water. In this paper we reserve the term "osmotic pressure" for actual pressures generated by osmosis, which generally are smaller than  $\pi$  because of osmotic efficiencies that are less than one.

[6] Like anomalous pressures generally, significant buildups of osmotic pressure are possible only in low-permeability settings or regions that are hydraulically isolated by low permeability barriers. Osmotic fluxes are small, and any permeable connection to normally pressured surroundings will prevent buildup of osmotic pressure. Depending on the pattern of solute concentration, osmosis can increase or decrease pressure, and thus either anomalously high or anomalously low pressures can result. In either case, osmosis occurs only where salinity gradients are present within semipermeable media or, in the present context, media containing significant clay. Porous media with little or no clay generally have no measurable osmotic properties and thus  $\sigma$  values of zero.

[7] Various situations conducive to osmotic pressures can be envisioned. Among the simplest is a low-permeability

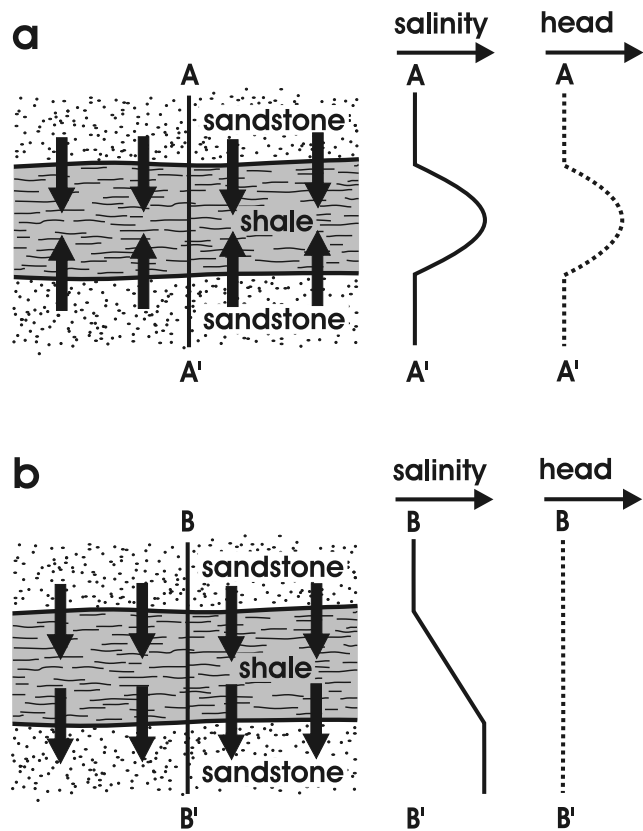


**Figure 1.** Examples of settings where osmotic fluxes and pressures might occur, showing profiles of salinity and hydraulic head. Bold black arrows show sense of osmotically driven flow, and the salinity and hydraulic head profiles are qualitative. (a) A situation where osmotically driven flow leads to buildup of osmotic pressure seen as excess hydraulic head. The anomalous osmotic pressures occur only within the low-permeability shale membrane. (b) A situation where osmotically driven flow causes no pressure buildup; the lower sandstone is not hydraulically isolated from its surroundings.

shale bounded by sandstones. If, for example, the shale and sandstones originally contain saline water and the sandstones are subsequently flushed with fresher water, concentration gradients will develop in the shale as solute diffuses into the sandstones and is advected away. If the shale behaves as a membrane, osmosis will drive fluid flow toward the highest concentration at the center of the shale, leading to anomalously high pressures there (Figure 1a). Likewise, if water in such a system is initially of low salinity, and high-salinity waters subsequently invade the sandstones, concentration gradients in the opposite direction will develop, and osmotic flow out of the shale will generate anomalously low pressures there. *Greenberg et al.* [1973] analyzed the latter scenario in a flow system near Oxnard, California, affected by seawater intrusion. In situations like that depicted in Figure 1a, the pressure anomalies are limited to the low-permeability shale membrane itself, where pressure measurements are difficult and seldom attempted. However, pressure anomalies will also exist in any sand lenses or stringers that happen to be present in the shale, and these are more readily detected.

[8] The situation in Figure 1a can be contrasted with that in Figure 1b. Here again a shale and adjoining sandstones originally contain saline water. If only one of the sandstones, say, the upper, is subsequently flushed with fresher water, a concentration gradient across the shale will develop. If the shale behaves as a membrane, osmosis will again drive flow toward high concentrations. In this case, however, the flow will be across the shale into the lower sandstone. Unless the lower sandstone is hydraulically isolated, no osmotic pressure buildup will occur.

### 3. Characterizing Argillaceous Membranes

[9] Unlike naturally occurring clay-rich formations, the membrane behavior of refined clays and other modified geologic materials has been studied experimentally for several decades because of its importance in engineering applications. For example, researchers have studied the osmotic properties of refined bentonite [Kemper, 1961; Fritz and Marine, 1983; Keijzer, 2000], kaolinite [Olsen, 1969] and smectite [Fritz and Whitworth, 1994], processed Pierre Shale [Kemper, 1961], harbor sludge [Keijzer, 2000], and geosynthetic liner media [Malusis and Shackelford, 2004]. Membrane behavior in these media is nearly always characterized by the osmotic efficiency  $\sigma$ , and determinations of  $\sigma$  have tended to rely on one of two approaches.

[10] Most commonly, a sample of the medium is placed between reservoirs containing solutions of different concentrations and the osmotic pressure is permitted to build up in the higher-concentration reservoir. The flow in the sample is one-dimensional and if, for simplicity, we consider the case where it is also horizontal, the component of  $\nabla z$  in the direction of flow is zero. Once osmotic pressure buildup has ceased ( $\mathbf{q} = 0$ ),  $\sigma$  can be calculated by integrating (1) to yield

$$\sigma = p_o / \Delta\pi, \quad (3)$$

where  $p_o$  is the equilibrium osmotic pressure [ $\text{ML}^{-1}\text{T}^{-2}$ ], or the final pressure difference between the reservoirs, and  $\Delta\pi$  is the difference in  $\pi$  in the reservoirs. This type of test is analogous to the subsurface osmotic system in Figure 1a.

[11] Alternatively, both reservoirs can be maintained at equal pressure and the flux  $\mathbf{q}$  can be measured after it has reached a steady state. In this case,  $p_o = 0$  and, if it is assumed that  $\mu$ ,  $k$ , and  $\sigma$  are constant, meaning  $\nabla\pi$  must also be constant across the sample,  $\sigma$  can be calculated after integrating and manipulating (1) to give

$$\sigma = (q\mu L / k\Delta\pi), \quad (4)$$

where  $L$  is the sample length. The osmotic system in Figure 1b is the subsurface analog of this type of test.

[12] Unfortunately, although  $\sigma$  has a simple physical interpretation and is easily calculated, it does not fully constrain a porous medium's osmotic behavior. In particular, it generally does not permit predicting osmotic pressures or fluxes under conditions differing from those of the test. This results from the fact that  $\sigma$  is not a property of the porous medium only, but is also strongly affected by solute concentration. Equations (3) and (4) are obtained by assuming  $\sigma$  does not vary across the sample. However, because osmosis occurs only when there is a concentration gradient in the membrane,

$\sigma$  generally will also vary spatially in the membrane. Values of  $\sigma$  calculated using (3) or (4) are actually apparent values that lie somewhere between the maximum and minimum  $\sigma$  in the sample during the experiment.

[13] Membrane characterization that will allow predicting osmotic pressures under various conditions must account for the strong dependence of  $\sigma$  on concentration. We can approach this problem by again considering a horizontally oriented sample of a semipermeable medium between reservoirs with different solute concentrations. If the sample-reservoir boundaries are at  $x = x_1, x_2$  and osmotic pressure has increased to an equilibrium value with  $\mathbf{q} = 0$ , integration of (1) between  $x_1$  and  $x_2$  with a concentration-dependent  $\sigma$  yields

$$\int_{x_1}^{x_2} \frac{dp}{dx} dx = \int_{x_1}^{x_2} \sigma(C) \frac{d\pi}{dx} dx. \quad (5)$$

A change of variable can be accomplished by noting that

$$\frac{d\pi}{dx} dx = \frac{d\pi}{dC} \frac{dC}{dx} dx = \frac{d\pi}{dC} dC, \quad (6)$$

which leads to

$$p_o = \int_{C_{\max}}^{C_{\min}} \sigma(C) \frac{d\pi}{dC} dC. \quad (7)$$

The left-hand side of (7) recognizes that the difference in pressure at  $x_1$  and  $x_2$  is the difference in pressure in the reservoirs or the osmotic pressure  $p_o$ . The right-hand side of (7) can be understood by imagining that finite-thickness membranes are composed of a sequence of thin subunits, each contributing a pressure increment determined by the concentration difference across it and the local value of  $\sigma$ .

[14] For a semipermeable porous medium in which  $\sigma(C)$  describes the dependence of  $\sigma$  on concentration, (7) is an expression for the equilibrium osmotic pressure generated by the concentration extremes  $C_{\max}$  and  $C_{\min}$ . It applies to subsurface systems as well as our hypothetical experiment. For example, if the concentration in the shale in Figure 1a is  $C_{\max}$  at its center and  $C_{\min}$  at its boundaries,  $p_o$  computed using (7) is the maximum excess pressure (shown as a head perturbation) at the center of the shale. Note that length ( $x$ ) does not appear in (7);  $p_o$  is determined by  $C_{\max}$  and  $C_{\min}$  and not the gradient in  $C$ .

[15] Quantitative models describing the dependence of  $\sigma$  on both medium properties and solute concentration have been developed for clays by a number of investigators, including Kemper and Rollins [1966], Groenevelt and Bolt [1969], Bresler [1973], and Marine and Fritz [1981]. All the models cited predict relationships between  $\sigma$  and  $C$  that are similar [Keijzer, 2000]. However, Bresler's [1973] model, which is a variant of Kemper and Rollins's [1966] model and is shown in Figure 2, offers certain advantages in the present context. First, as Bresler [1973] himself demonstrated, there is good agreement between  $\sigma$  values his model predicts and laboratory-determined  $\sigma$  values in a variety of processed clay media tested over a wide range of conditions (Figure 2a). Second, and of particular relevance here, Cey et al. [2001] found that measured  $\sigma$  values in cores of claystone from the

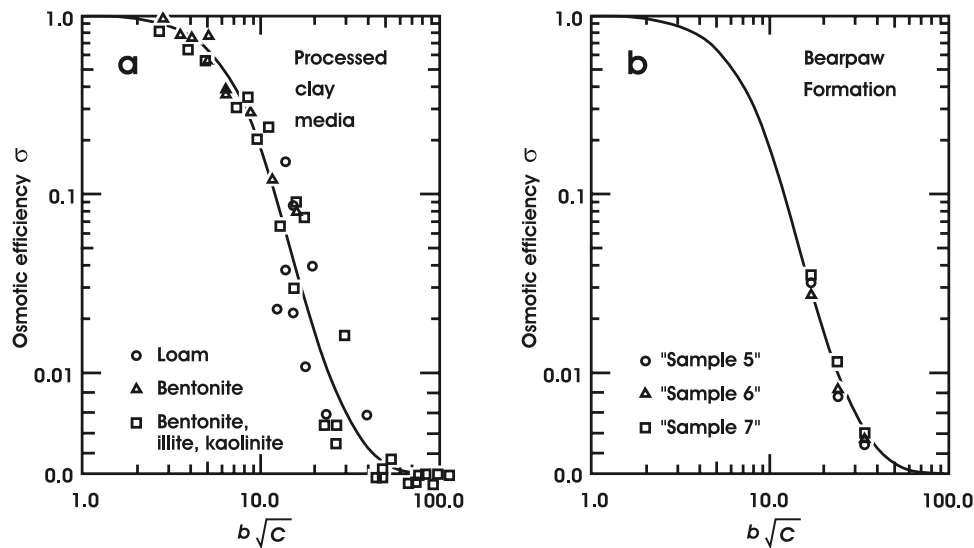


**Figure 2.** Osmotic efficiency  $\sigma$  as a function of  $b\sqrt{C}$  for monovalent solutes according to Bresler [1973] (solid curve in both plots).  $C$  is concentration expressed as normality, and  $b$  is the average half distance, in Å, between clay platelets forming pore throats. Note the linear vertical scale for  $\sigma$  below 0.01. (a) Comparison with experimental osmotic efficiencies in processed and refined clay media determined by Kemper and Rollins [1966], Letey et al. [1969], and Kemper and Quirk [1972] as compiled by Bresler [1973]. Data have been shifted laterally to improve fit by adjusting  $b$ . (b) Comparison with experimental osmotic efficiencies observed in core samples of claystone from the Bearpaw Formation and reported by Cey et al. [2001].

Bearpaw Formation are also well described by Bresler's model (Figure 2b). To our knowledge, no other model has been compared to the behavior of a geologic medium in its natural state. Although this offers no guarantee that Bresler's model is generally applicable in argillaceous formations, it makes it a logical choice for our analysis.

[16] A question might arise as to whether Bresler's model can be compared with experimental determinations of  $\sigma$  because the latter are effective values calculated using (3) or (4). Comparison is made possible by the fact that as the concentration difference imposed across the sample decreases, the error in the value of  $\sigma$  determined using (3) or (4) also decreases. The key is to use maximum and minimum experimental concentrations similar enough to make the error in  $\sigma$  acceptably small but also different enough that experimental noise is not a problem. Some of the data in Figure 2a are from Kemper and Rollins [1966], for example, who used concentrations that differed by a factor of 3 in each of their experiments, while the overall concentration range they examined in multiple experiments spanned 4 orders of magnitude. We estimate the resulting errors in the experimental  $\sigma$  values in Figure 2 are no more than a few percent.

[17] Bresler's [1973] model has an additional advantage for us of easily representing properties of different media. By plotting  $\sigma$  against  $b\sqrt{C}$ , where  $b$  [L] is the half width of the pores, Bresler found that the data for several different clay media clustered along a single curve, as seen in Figure 2. This "normalization" is possible because the product  $b^2 C$  is an important parameter in the nondimensional diffuse double layer equations [Mitchell, 1993] and because  $\sigma$  is only weakly dependent on the medium's surface charge density and the pore fluid's permittivity, which are the other controlling variables. This is discussed in greater detail in

Appendix A, where we outline the theory underpinning Bresler's [1973] model and critically evaluate the model itself.

[18] Figure 2 graphically illustrates the strong dependence of  $\sigma$  on both concentration and, through  $b$ , membrane pore size. The value of  $\sigma$  decreases as  $C$  increases, and clay media that are near-perfect membranes ( $\sigma \approx 1$ ) at low concentrations can exhibit almost no membrane properties ( $\sigma \approx 0$ ) at high concentrations. Conversely,  $\sigma$  can increase dramatically if a membrane is compacted and  $b$  decreases. Note that Figure 2 applies to monovalent solutes, such as NaCl, with a different curve [see Bresler, 1973] for divalent solutes.

[19] Bresler's relation between  $\sigma$  and  $b\sqrt{C}$  can be used in (7) to calculate equilibrium osmotic pressure  $p_o$  for any  $C_{\max}$  and  $C_{\min}$  if  $b$  is known. This suggests that determining  $b$  is a versatile way to characterize clay membranes because ideally at least, it is not influenced by solute concentration. However, an even more versatile metric can be derived from  $b$ . If the porosity of the medium is known,  $b$  can be used to calculate a quantity we call osmotic specific surface area and denote as  $A_{so}$  [ $L^2 M^{-1}$ ]. In principle,  $A_{so}$  is clay mineral surface area per unit mass of porous medium, an intrinsic property of the medium that is relatively invariant during compaction.

[20] An expression for  $A_{so}$  can be obtained by considering a highly idealized porous medium composed of parallel and evenly spaced clay platelets with  $b$  the half distance between the platelets. A basic unit of the medium (a unit that can be combined with other identical units to make an arbitrarily large mass of the medium) can be defined as a clay platelet together with half of the pore space on one side and half of the pore space on the other. If the area of the platelet is  $a$ , the total surface area in the unit is  $2a$ , counting both sides

of the platelet. The pore volume in the unit is  $ab$  on one side of the platelet and  $ab$  is on the other, or  $2ab$ , which is the total surface area multiplied by the pore half width  $b$ . Thus the pore volume per unit mass of this idealized porous medium is  $A_{so} b$ .

[21] In real argillaceous media, of course, clay particles and other mineral grains are arranged in a more complex fashion and the exact meaning of  $A_{so} b$  is less obvious (see Appendix A for further discussion). For our purposes, however, we simply define  $A_{so}$  as the pore volume per unit mass of porous medium divided by  $b$ , which leads to

$$A_{so} = \frac{n}{b\rho_b} = \frac{n}{b\rho_s(1-n)}, \quad (8)$$

where  $n$  is porosity [ $L^3 L^{-3}$ ], or pore volume per volume of medium,  $\rho_b$  is the medium dry bulk density [ $M L^{-3}$ ], and  $\rho_s$  is the mean solid grain density [ $M L^{-3}$ ]. Values of the latter are tabulated for various clay minerals by Mitchell [1993].

[22] Because of the nonideal arrangement of clay platelets in real clay media and to a lesser degree the approximations inherent in Bresler's curve,  $A_{so}$  is an effective rather than actual specific surface area. In particular, as we show in Appendix A, errors resulting from ignoring surface charge density and fluid permittivity are largely subsumed in the computed values of  $b$  and  $A_{so}$  and, in general, cause them to differ from their true values. We show below, however, that this contributes little error to our analysis.

[23] If it is assumed that  $A_{so}$  is indeed largely invariant during compaction (this is a crucial assumption discussed in more detail later),  $b$  can be calculated for any porosity from (8). When  $b$  is known,  $\sigma(C)$  is determined by Bresler's curve (Figure 2) and can be used in (7) to calculate the final osmotic pressure  $p_o$  for arbitrary values of  $C_{max}$  and  $C_{min}$ . This offers a way to characterize a clay medium's overall effectiveness as an osmotic membrane. In particular,  $A_{so}$  values permit comparison of osmotic tests conducted with different fluid concentrations and also permit prediction of  $p_o$  for any desired concentration range and membrane compaction state.

#### 4. New Data on Osmotic Properties

[24] Earlier we noted the historical lack of data on osmotic properties of unmodified geologic media. In contrast to the numerous studies of refined clays and other processed geomaterials, osmotic studies of geologic media in their natural state were virtually nonexistent until relatively recently. We are aware of only one fully described study prior to 2000, that of Young and Low [1965], who conducted tests on a Cretaceous siltstone. Two other studies described osmotic flows in shale samples [van Oort, 1994; van Oort et al., 1995] but did not report both maximum and minimum concentrations used in tests.

[25] Since results of an in situ osmosis test in the Pierre Shale were reported in 2000 [Neuzil, 2000], a number of osmosis tests on other argillaceous formations have been published. The data from these tests, and the values of  $A_{so}$  we computed from them, are presented in Table 1. The compilation includes a variety of lithologies, geologic ages, sampling depths, and testing styles. The motivations for obtaining the data in Table 1 are also varied, including evaluating repository sites for radioactive waste [Garavito et al., 2007; Noy et al., 2004], enhancing borehole stability

in shales [Al-Bazali, 2005; Rahman et al., 2005], and evaluating the role of membranes in groundwater systems [Neuzil, 2000; Cey et al., 2001; Garavito et al., 2006].

[26] Most of the tests compiled in Table 1 reported equilibrium osmotic pressure ( $p_o$ ), maximum and minimum concentrations ( $C_{max}$  and  $C_{min}$ ), and porosity ( $n$ ). The exceptions are Cey et al. [2001], who reported values of  $A_{so}$  directly, Garavito et al. [2007], who reported  $b$ , Young and Low [1965], who did not report porosity (we used a representative value for the formation), and Garavito et al. [2006, 2007], who analyzed osmotic pressure buildup as well as  $p_o$ . A representative temperature of 288 K (15°C) during the tests was used in our calculations, and except in the Boom Clay, the solute is NaCl.

[27] With the exceptions just noted,  $A_{so}$  values in Table 1 were calculated from test data using (7), with Bresler's  $\sigma$  versus  $b\sqrt{C}$  curve (Figure 2) used to specify  $\sigma(C)$  and the integration limits set at the experimental  $C_{max}$  and  $C_{min}$  values. First, values of  $b$  were obtained by trial-and-error matching of computed and observed  $p_o$ . Reported porosity values and estimated grain densities were then used in (8) to calculate  $A_{so}$ . The integral in (7) was evaluated numerically using a spline function fitted to tabulated  $\sigma$  versus  $b\sqrt{C}$  values obtained visually from Bresler's curve. A spline function was also fitted to tabulated  $a_w$  versus  $C$  values for NaCl [Robinson and Stokes, 2002] to calculate  $d\pi/dC$ . As in Bresler's analysis,  $C$  was expressed as normality. Numerical errors in the calculations are insignificant. We estimate errors from other sources in calculated values of  $b$  and  $A_{so}$  could be as much as a factor of 1.5 but are generally significantly less. A more detailed discussion of the computations and sources of error will be found in Appendix A.

[28] The in situ Pierre Shale test [Neuzil, 2000] yielded an  $A_{so}$  of  $\sim 40 \text{ m}^2 \text{ g}^{-1}$  (Table 1). Because of the unusually large smectite content of the Pierre, Neuzil [2000] argued that more effective osmotic membranes, or in this context formations with higher  $A_{so}$  values, are unlikely in nature. Apparently, that assertion is wrong. While  $A_{so}$  values for several formations in Table 1 are comparable to or smaller than that of the Pierre Shales ( $40\text{--}55 \text{ m}^2 \text{ g}^{-1}$ ), we were surprised to find that several formations have values that are significantly larger, with the largest approaching  $150 \text{ m}^2 \text{ g}^{-1}$ , or nearly 4 times that of the Pierre Shale. We can summarize by noting that the data in Table 1 suggest (1) the spectrum of osmotic properties in the subsurface is broad, encompassing membranes that are significantly more effective than anticipated, and (2) formations that can act as effective membranes are not rare.

[29] We were also surprised to find that there is little to indicate that the most smectite-rich formations are the best membranes, as would be anticipated from both theoretical considerations and experimental studies of modified clays [e.g., Kemper and Quirk, 1972; Marine and Fritz, 1981; Fritz, 1986]. The "ARCO China" Shale, for example, has a relatively large  $A_{so}$  ( $97 \text{ m}^2 \text{ g}^{-1}$ ) but contains relatively little smectite or mixed-layer clay (13%), while the smectite and mixed-layer clay-dominated Pierre Shale has an  $A_{so}$  roughly half as large ( $40\text{--}55 \text{ m}^2 \text{ g}^{-1}$ ). This is consistent with a similar lack of evidence for degradation of membrane capability with burial, compaction, and heating. Membrane effectiveness might be expected to be degraded by diagenetic conversion of smectite to illite with increasing temperature

Table 1. Values of Osmotic Specific Surface Area ( $A_{so}$ ) for Various Geologic Media<sup>a</sup>

| Age/Formation Name           | Lithology/Clay Mineralogy (%), <sup>b</sup> [CEC] (meq/100 g)              | Test or Sample Depth (m)/Porosity | Type of Test <sup>c</sup>      | Concentration Range During Test ( $g L^{-1}$ ) | Range in $\sigma$ During Test | Osmotic Pressure Generated (MPa) | $A_{so}$ ( $m^2 g^{-1}$ ) | Source   |
|------------------------------|--|-----------------------------------|--------------------------------|--|-------------------------------|----------------------------------|---------------------------|--|
| Oligocene/Boom Clay          | clay/C, 30–70; S, 10–30; ML, 5–50; I, 10–30; K, 1–30; CL, 1–5/[24]         | 223/0.38                          | in situ; transient pressure    | 0.850–8.50 <sup>d</sup>                        | 0.06–0.52                     | 0.020                            | 37 <sup>e</sup>           | Garavito <i>et al.</i> [2007] and Boisson [2005] |
| Cretaceous/Pierre Shale      | claystone/C, 70–80; ML, 80/[20–50]   | 75/0.34                           | in situ; equilibrated pressure | 3.50–6.52                                      | 0.038–0.14                    | 0.0146–0.0216                    | 40                        | Neuzil [2000] and Schultz <i>et al.</i> [1980]   |
| Cretaceous/Pierre Shale      | claystone/C, 70–80; ML, 80/[20–50]   | 75/0.34                           | in situ; transient pressure    | 3.50–6.52                                      | 0.038–0.14                    | 0.0146–0.0216                    | 46                        | Garavito <i>et al.</i> [2006]                    |
| Cretaceous/Pierre Shale      | claystone/C, 64; S, 17; ML, 49; I, 19; CL, 4/[10.5]                        | Outcrop/0.26                      | lab; equilibrated pressure     | 35.2–115.0                                     | 0.0051–0.025                  | 0.083                            | 55                        | Al-Bazali [2005]                                 |
| Cretaceous/Bearpaw Formation | claystone/C, 57; S, 50–60; I, 10–20  | 88 and 123/0.38–0.43              | lab; equilibrated flow         | 4.0–8.0 8.0–16.0 16.0–33.0                     | 0.0028–0.42                   | NA                               | 45–79                     | Cey <i>et al.</i> [2001]                         |
| Cretaceous/Viking Formation  | siltstone/C, 8–12; S and ML, 8–22; I, 40–50; K, 30–40                      | 1500/0.14 <sup>f</sup>            | lab; equilibrated pressure     | 0.005 <sup>g</sup> –61.4                       | 0.001–1.0                     | 0.014–0.028                      | 4                         | Young and Low [1965]                             |
| Cretaceous/Viking Formation  | siltstone/C, 8–12; S and ML, 8–22; I, 40–50; K, 30–40                      | 1500/0.14 <sup>f</sup>            | lab; equilibrated pressure     | 61.4–128.7                                     | 0.0004–0.0012                 | 0.0035–0.0069                    | 9                         | Young and Low [1965]                             |
| Jurassic/Opalinus Clay       | calcareous claystone/C, 28–93; ML, 5–20; I, 15–30; K, 15–37; CL, 3–18/[11] | 250–320/0.16                      | in situ; equilibrated pressure | 0.01 <sup>g</sup> –18.9                        | 0.003–1.0                     | 0.081                            | 10                        | Noy <i>et al.</i> [2004] and Boisson [2005]      |
| Jurassic/Opalinus Clay       | calcareous claystone/C, 28–93; ML, 5–20; I, 15–30; K, 15–37; CL, 3–18/[11] | 250–320/0.16                      | in situ; equilibrated pressure | 18.9–87.5                                      | 0.0078–0.087                  | 0.152                            | 31                        | Noy <i>et al.</i> [2004] and Boisson [2005]      |
| Jurassic/Opalinus Clay       | calcareous claystone/C, 28–93; ML, 5–20; I, 15–30; K, 15–37; CL, 3–18/[11] | 250–320/0.16                      | lab; equilibrated flow         | 0.005 <sup>g</sup> –14.3                       | 0.0044–1.0                    | 0.073 <sup>i</sup>               | 10                        | Noy <i>et al.</i> [2004] and Boisson [2005]      |
| Jurassic/Opalinus Clay       | calcareous claystone/C, 28–93; ML, 5–20; I, 15–30; K, 15–37; CL, 3–18/[11] | 250–320/0.16                      | lab; equilibrated flow         | 0.005 <sup>g</sup> –14.3                       | 0.0026–1.0                    | 0.054 <sup>i</sup>               | 8                         | Noy <i>et al.</i> [2004] and Boisson [2005]      |
| Jurassic/Opalinus Clay       | calcareous claystone/C, 28–93; ML, 5–20; I, 15–30; K, 15–37; CL, 3–18/[11] | 250–320/0.16                      | lab; equilibrated flow         | 0.005 <sup>g</sup> –14.3                       | 0.0011–1.0                    | 0.019 <sup>i</sup>               | 5                         | Noy <i>et al.</i> [2004] and Boisson [2005]      |
| /'C1'' Shale                 | shale/C, 76; K, 39/[21]  | 2100/0.28                         | lab; equilibrated pressure     | 35.2–218.2                                     | 0.0033–0.044                  | 0.207                            | 72                        | Al-Bazali [2005]                                 |
| /'C1'' Shale                 | shale/C, 70; K, 26/[23]  | 2100/0.28                         | lab; equilibrated pressure     | 35.2–115.0                                     | 0.0088–0.053                  | 0.159                            | 76                        | Al-Bazali [2005]                                 |
| /'C2'' Shale                 | shale/C, 70; K, 26/[23]  | 2700/0.13                         | lab; equilibrated pressure     | 35.2–115.0                                     | 0.011–0.077                   | 0.220                            | 32                        | Al-Bazali [2005]                                 |
| /'C2'' Shale                 | shale/C, 70; K, 26/[23]  | 2700/0.13                         | lab; equilibrated pressure     | 35.2–218.2                                     | 0.0050–0.077                  | 0.331                            | 32                        | Al-Bazali [2005]                                 |
| /'ARCO China'' Shale         | shale/C, 31; S, 13; I, 44; K, 14; CL, 10/[24.5]                            | 3800/0.21                         | lab; equilibrated pressure     | 115.0–218.2                                    | 0.020–0.060                   | 0.481                            | 97                        | Al-Bazali [2005]                                 |
| /'Shale ''W''                | /[20.5]  | /0.142                            | lab; equilibrated pressure     | 57.6–174.2                                     | 0.41–0.76                     | 7.70                             | 142 <sup>h</sup>          | Rahman <i>et al.</i> [2005]                      |

<sup>a</sup>The solute in all tests was NaCl except where noted.  
<sup>b</sup>C, total clay; S, smectite; ML, mixed layer smectite/illite; I, illite; K, kaolinite; CL, chlorite.  
<sup>c</sup>Only the equilibrium or maximum osmotically generated pressure is considered in "equilibrated pressure" tests, whereas the pressure buildup is also analyzed in "transient pressure" tests. "Equilibrated flow" test results are based on the equilibrated osmotically generated fluid flux when pressure is not permitted to build up.  
<sup>d</sup>NaHCO<sub>3</sub> is dominant solute.  
<sup>e</sup>Computed from porosity and reported value for  $b$  of 61 Å.  
<sup>f</sup>Average porosity of Viking Formation as reported by Bekele *et al.* [2002].  
<sup>g</sup>Estimated concentration shortly after test section flushed with distilled water.  
<sup>h</sup>Test conducted under 27.6 MPa confining pressure. Smaller osmotic pressures were obtained under lower confining loads, suggesting sample was microfractured, probably during coring.  
<sup>i</sup>Computed values for test conditions.

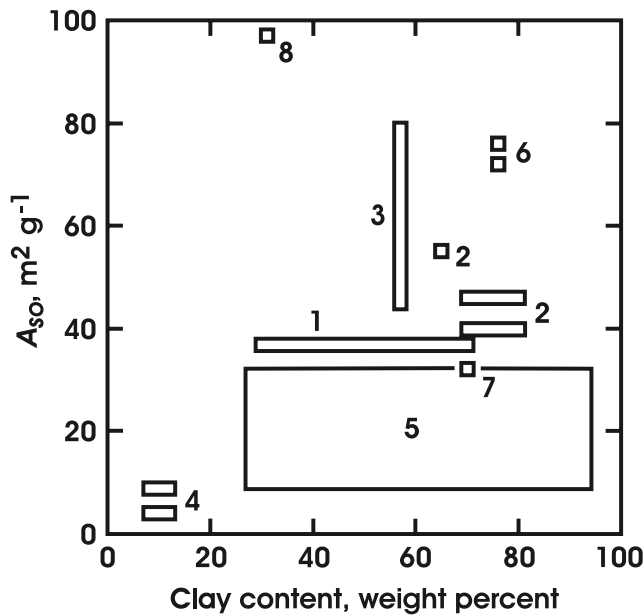


**Figure 3.** Relation between osmotic specific surface area ( $A_{so}$ ) and weight percent clay of certain formations in Table 1. Numeral 1 is Boom Clay, 2 is Pierre Shale, 3 is Bearpaw Formation, 4 is Viking Formation, 5 is Opalinus Clay, 6 is “C1” Shale, 7 is “C2” Shale, and 8 is “ARCO China” Shale.

and pressure, but three of the largest tabulated  $A_{so}$  values (72, 76, and  $97 \text{ m}^2 \text{ g}^{-1}$ ) were obtained from two of the deepest core samples (the “C1” Shale from 2.1 km and the “ARCO China” Shale from 3.8 km). We suspect that the influence of clay mineralogy has been overwhelmed by differences in the microstructure of these media and that these differences are related to their depositional environments.

[30] Degree of compaction does not show a systematic relation to  $A_{so}$  either; the medium with the smallest reported porosity (the “C2” Shale at 0.13) has a middling  $A_{so}$  of  $32 \text{ m}^2 \text{ g}^{-1}$ . However, one trend that is discernible in the data is that of increasing  $A_{so}$  with clay content. This can be seen in Figure 3, a plot of  $A_{so}$  versus clay content for the formations in Table 1. However, conspicuous exceptions exist even here; the “ARCO China” Shale (region 8) has a higher than expected  $A_{so}$  value for its reported clay content, while some tests in the Opalinus Clay (region 5) yielded  $A_{so}$  values smaller than expected for its reported clay content. The reason for these outliers is not clear but may also be related to microstructure.

[31] Do the data in Table 1 show the full range of membrane properties in the subsurface? This is an important question in view of the relatively small number of data available. The answer appears to be “no” when  $A_{so}$  values from Table 1 are compared with other measures of specific surface area in argillaceous media. Figure 4 reproduces a plot by Patchett [1975] of specific surface area measured using glycol retention ( $A_{sg}$ ) versus bulk cation exchange capacity (CEC) for a large number of shales (solid dots). Patchett’s data show a well-defined trend of increasing  $A_{sg}$  with CEC. Where CEC values are available for formations in Table 1, we have added the corresponding  $A_{so}$  data to the plot. It appears that the  $A_{so}$  data in Table 1 span much, but not all of the range of CECs observed in argillaceous

formations. Figure 4 suggests a more extensive set of data would include both smaller and larger  $A_{so}$  values at the lower and upper ranges of CEC. In the case of the latter,  $A_{so}$  values as large as  $\sim 200 \text{ m}^2 \text{ g}^{-1}$  appear likely in media with CEC values of 60–70 meq/100 g.

[32] Almost all of the  $A_{so}$  values are smaller than  $A_{sg}$  values for comparable CECs, and some are significantly smaller. The discrepancy probably arises from several causes, including the fact that surface charge density is not explicitly accounted for in Bresler’s [1973]  $\sigma$  versus  $b\sqrt{C}$  curve. If the surface charge density used to generate the  $\sigma$  versus  $b\sqrt{C}$  curve is too small, the computed value of  $A_{so}$  will also be too small (see equation (A13) and the accompanying discussion in Appendix A). However, this is insufficient to explain the larger differences between  $A_{so}$  and  $A_{sg}$ . Another possible cause is that  $A_{so}$  is an osmotic flow-related property. Flow bypasses dead-end pores in clays [see, e.g., Olsen, 1962], reducing the surface area that influences it and perhaps leading to computed effective surface areas that are too small. Error and ambiguity in porosity values may also play a role. These uncertainties do not alter the likelihood of formations with both smaller and larger  $A_{so}$  values than so far measured.

## 5. Implications for Anomalous Subsurface Pressures

[33] To better gauge the implications of the new data, we constructed plots of equilibrium osmotic pressure  $p_o$  that

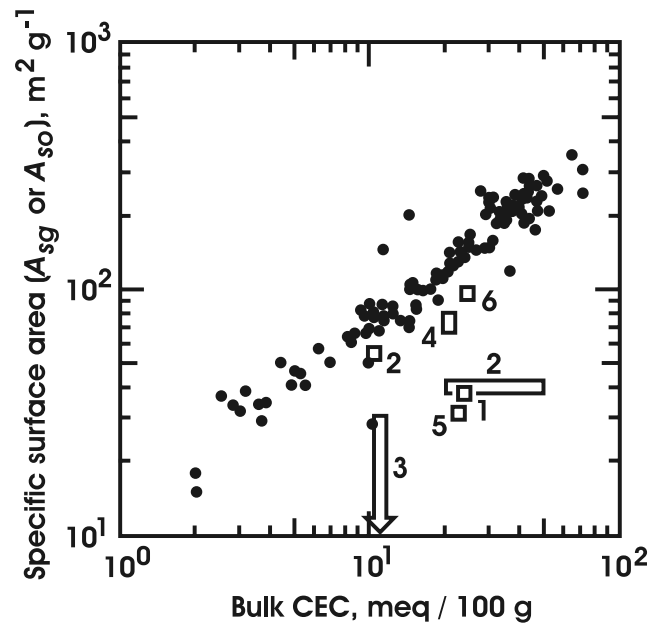


**Figure 4.** Relation between cation exchange capacity (CEC) and specific surface area in shales and claystones. Solid dots are Patchett’s [1975] data on specific surface area measured using glycol retention ( $A_{sg}$ ) for shale cores from California, Louisiana, Oklahoma, and Wyoming. Numbered data are osmotic specific surface area ( $A_{so}$ ) values from Table 1 where 1 is Boom Clay, 2 is Pierre Shale, 3 is Opalinus Clay, 4 is “C1” Shale, 5 is “C2” Shale, and 6 is “ARCO China” Shale. The arrow shape for region 3 is a reminder that two of the calculated  $A_{so}$  values for the Opalinus Clay (8 and  $5 \text{ m}^2 \text{ g}^{-1}$ ) are too small to show in the plot.

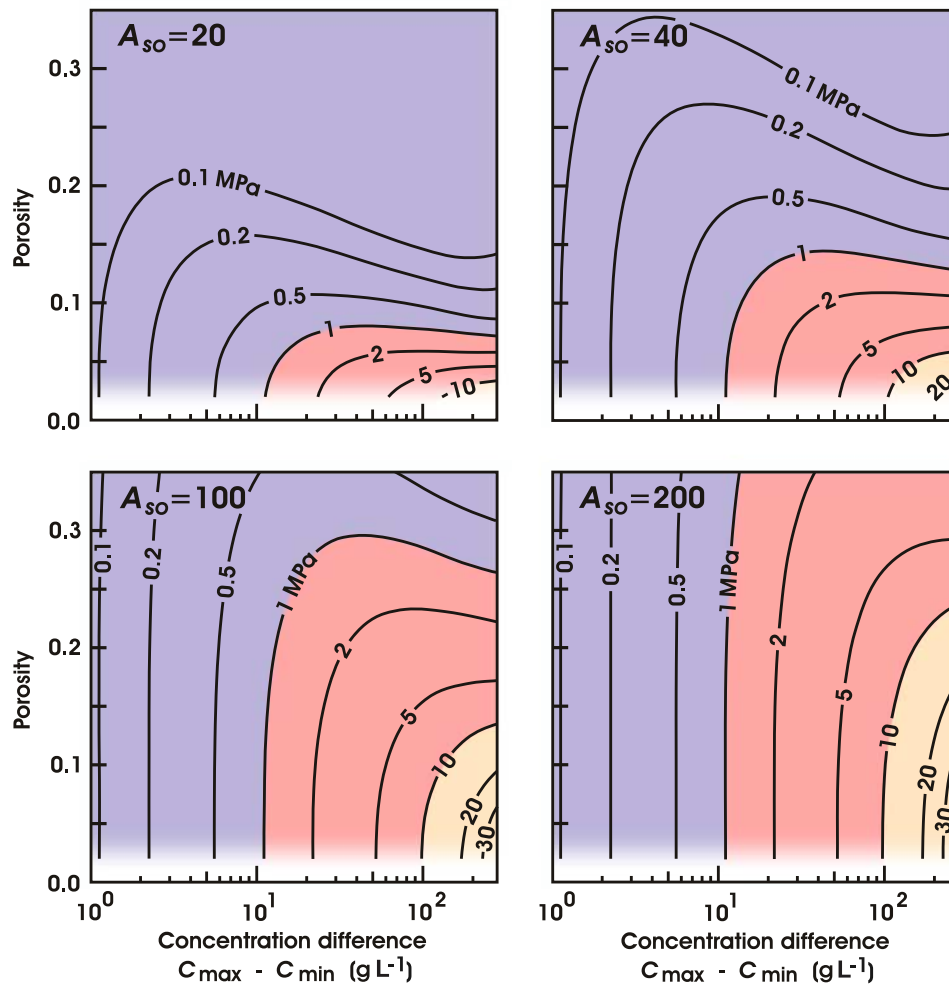


**Figure 5.** Equilibrium osmotic pressure  $p_o$  in MPa as a function of porosity and concentration difference for  $A_{so}$  values of 20, 40, 100, and 200  $\text{m}^2 \text{g}^{-1}$  when  $C_{\min}/C_{\max} = 0.1$ . To construct the plot, values of  $b$  were calculated from porosity using equation (8) and used to specify  $\sigma(C)$  from Bresler's [1973] curve assuming a monovalent solute (NaCl) (see Figure 2). Pressures were then calculated using equation (7) with  $R = 8.31 \text{ m}^3 \text{ Pa mol}^{-1} \text{ K}^{-1}$ ,  $V_w = 1.8 \times 10^{-5} \text{ m}^3 \text{ mol}^{-1}$ ,  $T = 288 \text{ K}$ , and  $\rho_s = 2.79 \text{ g cm}^{-3}$ . Porosities below  $\sim 0.03$  are considered unrealistic.

could be generated by membranes with  $A_{so}$  values of 20, 40, 100, and 200  $\text{m}^2 \text{g}^{-1}$  for ranges of porosity and concentration difference ( $C_{\max} - C_{\min}$ ) we consider reasonable for the subsurface. Equilibrium osmotic pressure  $p_o$  was computed as follows: After choosing porosity  $n$ ,  $b$  was calculated for the appropriate  $A_{so}$  and (7) was numerically integrated between the limits  $C_{\max}$  and  $C_{\min}$  using Bresler's  $\sigma$  versus  $b\sqrt{C}$  curve.

[34] Constructing the plots is complicated by the fact that  $p_o$  depends not only on the concentration difference ( $C_{\max} - C_{\min}$ ), but also on the actual values of  $C_{\max}$  and  $C_{\min}$ . For example, the osmotic pressure generated by a  $C_{\max}$  of 2  $\text{g L}^{-1}$  and a  $C_{\min}$  of 1  $\text{g L}^{-1}$  (a difference of 1  $\text{g L}^{-1}$ ) will be larger than the osmotic pressure generated by a  $C_{\max}$  of 20  $\text{g L}^{-1}$  and a  $C_{\min}$  of 19  $\text{g L}^{-1}$  (also a difference of 1  $\text{g L}^{-1}$ ) because of the overall decrease in  $\sigma$  as concentration increases. Thus we constructed plots for two scenarios:  $C_{\min}/C_{\max} = 0.1$  and  $C_{\min}/C_{\max} = 0.5$ . Specifying both  $C_{\min}/C_{\max}$  and  $C_{\max} - C_{\min}$  fully constrains the computations. The resulting plots are presented as Figures 5 and 6.

[35] Figure 5 shows the plots for  $C_{\min} = 0.1 C_{\max}$ , representing what we consider the largest concentration contrasts likely to occur naturally in subsurface membrane units. It implies osmosis in nature can generate osmotic pressures in excess of 30 MPa, the equivalent of approximately 3 km of hydraulic head, for  $A_{so}$  values of 100  $\text{m}^2 \text{g}^{-1}$  and 200  $\text{m}^2 \text{g}^{-1}$ . For the former, the medium must be compacted to relatively low porosities to achieve such large pressures,  $\sim 0.07$  or less, while for the latter porosity can be as large as  $\sim 0.12$ . The plots suggest that somewhat smaller maximum osmotic pressures of 10–20 MPa are attainable with  $A_{so}$  values of 20  $\text{m}^2 \text{g}^{-1}$  and 40  $\text{m}^2 \text{g}^{-1}$ , but require quite low porosities ( $\sim 0.03$ ). For  $A_{so}$  values of 100  $\text{m}^2 \text{g}^{-1}$  and 200  $\text{m}^2 \text{g}^{-1}$ , however, 10 MPa may be attainable at porosities as large as  $\sim 0.14$  and  $\sim 0.23$ , respectively. To place these pressures in perspective, we note that excess pressures in the neighborhood of 50 MPa are often encountered during hydrocarbon exploration, and values as high as 70 or even 80 MPa have been extrapolated from mud weight data [e.g., Spencer, 1994]. However, most anomalous pressures fall

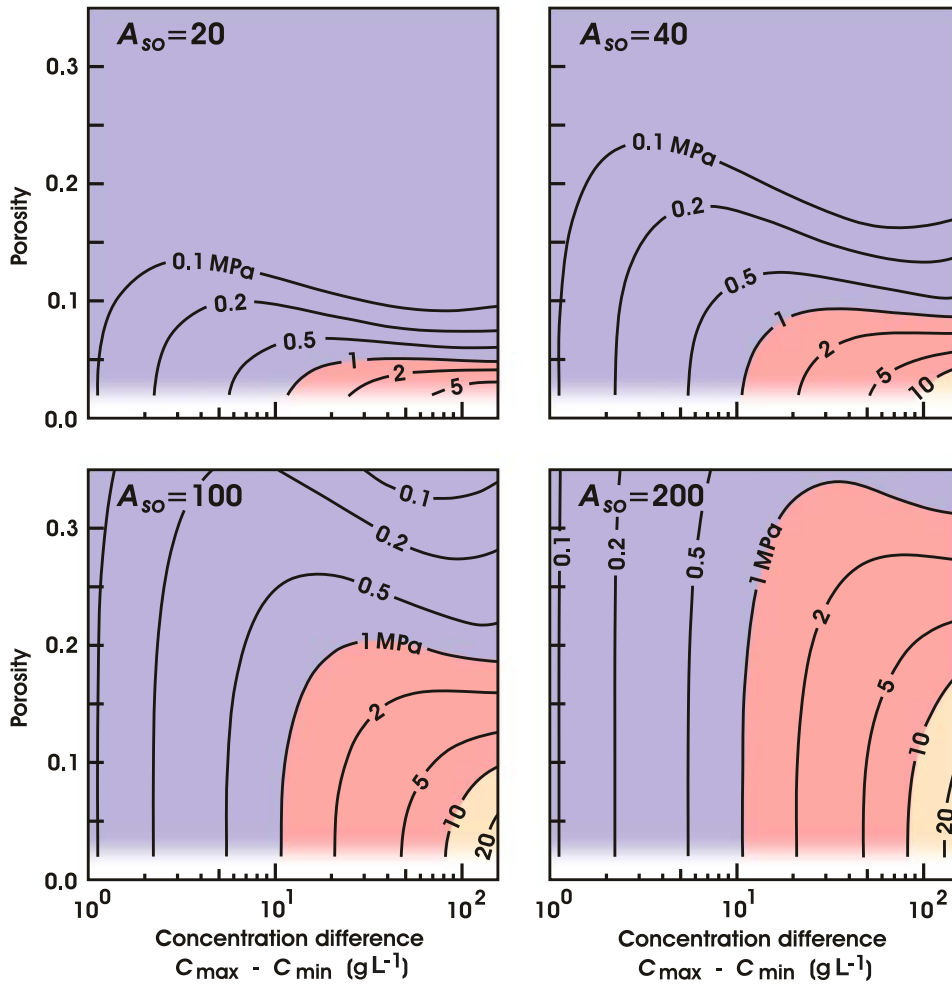


**Figure 6.** Equilibrium osmotic pressure  $p_o$  in MPa as a function of porosity and concentration difference for  $A_{so}$  values of 20, 40, 100, and 200  $\text{m}^2 \text{g}^{-1}$  when  $C_{\min}/C_{\max} = 0.5$ . The plots assume the same solute properties and parameter values as Figure 5 and were constructed in a similar manner. Porosities below  $\sim 0.03$  are considered unrealistic.

within the 30 MPa and smaller range our analysis suggests can be attained by osmosis.

[36] The Pierre Shale experiment [Neuzil, 2000], which yielded an  $A_{so}$  of  $\sim 40 \text{ m}^2 \text{g}^{-1}$ , implied that argillaceous media must be compacted to small porosities to attain large osmotic pressures (Figure 5;  $A_{so} = 40 \text{ m}^2 \text{g}^{-1}$ ). This significantly limited the environments in which large osmotic pressure anomalies might be expected.  $A_{so}$  values up to  $200 \text{ m}^2 \text{g}^{-1}$  imply much less compaction is required (Figure 5), and significantly broaden the range of environments that might be expected to host osmotic pressures.

[37] Figure 6 shows the case of  $C_{\min} = 0.5 C_{\max}$ , representing a less dramatic contrast in concentration. Predicted osmotic pressures are smaller than for  $C_{\min} = 0.1 C_{\max}$ , but still substantial. In particular, we note that osmotic pressures of  $\sim 20$  MPa are still predicted for porosities as large as  $\sim 0.10$  and pressures of  $\sim 10$  MPa for porosities as large as  $\sim 0.17$  for an  $A_{so}$  of  $200 \text{ m}^2 \text{g}^{-1}$ .

[38] The results in Figures 5 and 6 should be treated as scoping calculations subject to error and uncertainty from various sources. As discussed in Appendix A, scatter in the laboratory data in Figure 2a suggests errors in  $\sigma$ , and thus in predicted  $p_o$ , as great as a factor of  $\sim 3$  are possible.

However, errors of this type in our analyses are likely to be substantially smaller because in essence, we are fitting each experimental measurement in Table 1 to Bresler's curve. Graphically, this is equivalent to translating the data along the  $b\sqrt{C}$  axis to fit it to the curve.

[39] A potentially more important source of error, and one that is difficult to assess, is our assumption that Bresler's  $\sigma$  versus  $b\sqrt{C}$  curve describes the osmotic behavior of all the media in Table 1. Although behavior observed in the Bearpaw Formation is well described by Bresler's curve for the range of conditions Cey *et al.* [2001] tested (Figure 2b), general applicability of the Bresler model to argillaceous media in their natural state has not been demonstrated. Nevertheless, Table 1 provides some important insights in this regard. We note that calculated  $A_{so}$  values range from 5 to  $31 \text{ m}^2 \text{g}^{-1}$  for five experiments in the Opalinus Clay (Table 1). This may reflect inapplicability of the Bresler curve in the Opalinus, which is a calcareous claystone. In contrast,  $A_{so}$  values from experiments with different concentration ranges in both the "C1" and "C2" Shales (Table 1) are identical or nearly so, suggesting Bresler's curve is appropriate in those formations, which are shales or claystones.

[40] Finally, we note that the plots in Figures 5 and 6 rely on the potentially problematic assumption that  $A_{so}$  is invariant during burial and compaction of sediments. At least two compaction mechanisms, creation of inaccessible and dead-end pores by closure of pore throats and increase in direct contact area between clay platelets, and two diagenetic mechanisms, illitization of smectite clays and precipitation of nonclay minerals, may decrease  $A_{so}$ . If decreases occur and are significant, the large osmotic pressures we predict for membranes with large  $A_{so}$  values at low porosities are not really attainable. This possibility should be tempered by recalling there does not appear to be any trend in  $A_{so}$  values with either burial depth or porosity in the data.

## 6. What Do the Results Mean?

[41] We have already made the observation that the new data significantly broaden the conditions previously suggested [Neuzil, 2000] for generating osmotic pressures, and they imply that effective geologic membranes are not rare. Nevertheless, the notion of osmotically generated pressures in the subsurface is usually greeted skeptically [e.g., Bradley, 1975; Gretener, 1981; Domenico and Schwartz, 1990; Osborne and Swarbrick, 1997], and few, if any, groundwater regimes seem to offer compelling examples of osmotically generated pressures. We are aware of only two pressure regimes that are difficult to explain except as natural osmotic systems: anomalously high pressures in shales of the Triassic Dunbarton Basin, eastern United States [Marine, 1974; Marine and Fritz, 1981], and in an argillite in the eastern Paris Basin, France [Gueutin et al., 2007]. The Dunbarton Basin has coincident regions of elevated salinity and fluid pressure and lacks other plausible pressuring mechanisms, such as active compaction or high elevation recharge. The Callovo-Oxfordian argillite in the eastern Paris Basin exhibits hydraulic heads  $\sim 50$  m higher than in overlying and underlying strata, appears to have elevated salinity, and also appears to lack other plausible pressuring mechanisms.

[42] Why is our analysis seemingly at odds with field observations? We offer three hypotheses:

[43] 1. Our analysis is flawed, and geologic membranes are less efficient and/or less common than it suggests. Certain assumptions used in the analysis may not hold. These include the applicability of Bresler's [1973] osmotic efficiency model. It is based on the Kemper and Rollins [1966] model which appears to be conceptually flawed and is itself based on rather restrictive assumptions (see Appendix A). Perhaps the most crucial and potentially troublesome assumption, however, is that  $A_{so}$  is invariant during burial and compaction. If burial and diagenesis decrease  $A_{so}$ , it may not be possible to attain osmotic pressures as large as those in Figures 5 and 6.

[44] While there are certainly potential flaws in our analysis, however, they do not seem to offer a full explanation for the rarity of reported osmotic pressures in the field. Osmotic pressures of  $\sim 8$  MPa (large enough to be considered significant in many settings) have been generated by a shale in a laboratory test (shale "W" in Table 1 [Rahman et al., 2005]). This simple observation invokes no assumptions. Thus even if argillaceous formations are not able to generate osmotic pressures as large as our analysis indicates, it is clear that they can generate osmotic pressures large enough

to be noticed. Indeed, 8 MPa dwarfs the subsurface anomalies interpreted as possible osmotic pressures by Marine and Fritz [1981] ( $\sim 1$  MPa) and Gonçalves et al. [2004] ( $\sim 0.4$  MPa).

[45] 2. Osmotic pressures are rare because the conditions they require are rare. Large differences in solute concentration are present in many basins, which often contain relatively fresh meteoric waters at shallow depths and brines at greater depths. Most basins also contain abundant clay-rich strata. However, these factors by themselves are not sufficient for osmotic pressures to be generated. Concentration differences must be present within clay-rich sequences for osmotic fluxes to occur. Osmotic fluxes, moreover, can generate pressures only in low-permeability units or units that are hydraulically isolated by low-permeability barriers. The combined salinity patterns, stratigraphic configurations, and permeability regimes necessary to generate large osmotic pressures may simply be rare.

[46] It is also possible that argillaceous formations that are effective membranes in tests are ineffective at larger scales. The experimental data in Table 1 were obtained at scales ranging from  $\sim 10^{-2}$  m for lab tests to as much as  $\sim 10^1$  m for in situ tests. In contrast, observed concentration patterns in clay-rich formations suggest dimensions of  $\sim 10^1$  to  $\sim 10^4$  m for subsurface osmotic systems. For example, Hendry and Schwartz [1988] documented systematic changes in pore water concentration in a 100-m vertical section of Colorado Formation claystone in Alberta, Canada. Other examples include the Dunbarton Basin, in which the clay-rich fill with distinct concentration gradients extends about 1 km vertically and about 5 km laterally [Marine and Fritz, 1981], and the Paris Basin [Gonçalves et al., 2004; Gueutin et al., 2007], where the argillite hosting regular concentration changes is  $\sim 100$  m thick. If an argillaceous formation is pervaded by transmissive fractures, experiments may not be indicative of behavior on these scales, because the fractures could permit solute leakage and short-circuit osmotic pressure buildup. Tempering this possibility, however, is the observation that many argillaceous formations exhibit similar permeabilities at both small and large scales, indicating that short-circuiting is absent [Neuzil, 1994].

[47] 3. Investigators have not looked in the right places or have not recognized osmotic pressures when they are encountered. Osmotic pressures may be largely confined to argillaceous units or sequences dominated by argillaceous units. Fluid pressure measurements are rarely attempted in these environments and, even when they are, often do not yield indicative results. The supposed osmotic pressures in the Dunbarton Basin reported by Marine and Fritz [1981], for example, were discovered only after careful monitoring over several years to determine the pressure regime in the basin shales.

[48] If detected, osmotic pressures may well be misinterpreted. Poorly constrained geologic histories together with complex permeability, concentration, and pressure patterns in the subsurface often make it difficult to discriminate between multiple explanations for pressure anomalies. We also suspect that skepticism may lead investigators to ignore osmosis when interpreting subsurface fluid pressure regimes.

## 7. Conclusions

[49] Anomalous pressures reveal two things about their geologic environment: First, it is sufficiently isolated

hydraulically to permit slow forcing to cause pressure to build up. Second, one or more processes, operating now or in the past, supplied energy to create the pressure anomaly. The role of osmosis in generating anomalous pressures takes on particular significance when one is interested in the latter. Nonosmotic anomalies are generated by a dynamic process such as tectonic deformation, compaction, diagenesis, or heating. As such, they may reveal otherwise undetectable processes [e.g., *van Ruth et al.*, 2003] and can help constrain their rates. In contrast, osmotic pressure anomalies are not indicators of any dynamic geologic process. Rather, they are generated by chemical potential differences. Misidentification of the origin of an anomaly can lead to misinterpretation of the flow regime, its geologic setting, and its history.

[50] Geological osmosis may be a concern in specialized characterization efforts, such as siting radioactive waste repositories, for this reason. Long-term isolation of wastes is best assured by a thorough understanding of the history and nature of preexisting flow regimes. Globally, a number of candidate repository sites are in argillaceous formations that may be capable of hosting osmotic pressures.

[51] Better understanding of geological membranes and their ability to generate osmotic pressures will require more extensive experimental characterization of their properties than has been attempted thus far. An important step will be improved characterization of the functional dependence of  $\sigma$  on  $C$  in formations of interest. This will require experimentally characterizing  $\sigma$  at various concentrations. Formations may be heterogeneous with respect to their osmotic properties, complicating characterization. Better understanding of  $A_{so}$  as a measure of membrane effectiveness is also desirable. In particular, the assumed invariance of  $A_{so}$  during compaction and when exposed to solute concentration changes should be examined experimentally. Finally, it is desirable to extend the range of experimentally generated pressures to values comparable to the largest predicted, i.e., 20–30 MPa. The ability of geologic membranes to generate such large pressures is, at present, a theoretical extrapolation. Attaining osmotic pressures of 20–30 MPa in the laboratory will be technically challenging, however, because of the greatly increased tendency for leaks in the test apparatus and around the sample.

[52] In closing, we note that although further experimental characterization is important, understanding the significance of geological osmosis probably will require identifying compelling examples in the subsurface. To this end, investigators should be alert to the possibility of osmotic pressuring and aware of the conditions that favor it.

## Appendix A: Outline of Bresler's Osmotic Efficiency Model

[53] Like other models of osmotic efficiency in clay media, *Bresler's* [1973] model recognizes that the electrical potential field generated by negative charges on clay surfaces extends into the pore space and, in sufficiently small pores, restricts the flow of ions. The strength of the potential field and degree of ionic restriction increases with increasing clay surface charge density and decreases with increasing solute concentration and with distance from the clay surface. A conceptual basis for analyzing how the electric potential field controls osmotic efficiency is provided by diffuse double

layer theory. A useful overview of the latter is given by *Mitchell* [1993].

[54] Diffuse double-layer theory is usually developed for pores or pore throats idealized as openings between parallel clay platelets which permits solving the double layer equations in one dimension. *Bresler* [1970] gives the Poisson-Boltzmann equation for electrical potential between parallel charged clay surfaces in the presence of a single, symmetrical electrolyte as

$$\left[ \frac{d(\nu \hat{\Psi})}{dy} \right]^2 = \left( \frac{8 \pi N_A^2 e^2 \nu C}{D R T} \right) \cdot [2 \cosh(\nu \hat{\Psi}) - 2 \cosh(\nu \hat{\Psi}_b)], \quad (A1)$$

where  $\hat{\Psi}$  is a nondimensional electrical potential,  $\nu$  is ion valence [dimensionless],  $N_A$  is Avogadro's number [ $\text{mol}^{-1}$ ],  $e$  is the charge on an electron [Q],  $C$  is anion concentration in the bulk solution [ $\text{mol L}^{-3}$ ],  $D$  is relative permittivity of the pore water [ $\text{Q}^2 \text{T}^2 \text{M}^{-1} \text{L}^{-3}$ ],  $R$  is the general gas constant [ $\text{M L}^2 \text{T}^{-2} \Theta^{-1} \text{mol}^{-1}$ ],  $T$  is temperature [ $\Theta$ ], and  $y$  is the coordinate normal to the clay surfaces [L]. Nondimensional electrical potential is  $\hat{\Psi} = e N_A \Psi / (R T)$ , where  $\Psi$  is electrical potential [ $\text{M L}^2 \text{T}^{-2} \text{Q}^{-1}$ ]. The boundary condition for (A1), which follows from electroneutrality, is given by *Bresler* [1970] as

$$\cosh(\nu \hat{\Psi}_S) - \cosh(\nu \hat{\Psi}_b) = \frac{\pi \Gamma_S^2}{D R T C}, \quad (A2)$$

where  $\hat{\Psi}_b$  is the nondimensional electrical potential at the midplane between the clay surfaces (that are  $2b$  apart),  $\hat{\Psi}_S$  is the nondimensional electrical potential at the clay surface, and  $\Gamma_S$  is the clay's effective surface charge density [ $\text{Q L}^{-2}$ ]. For a monovalent solute ( $\nu = 1$ ), (A1) and (A2) simplify somewhat and can be written in fully nondimensional form as

$$\left( \frac{d\hat{\Psi}}{d\hat{y}} \right)^2 = \hat{C} [\cosh(\hat{\Psi}) - \cosh(\hat{\Psi}_b)] \quad (A3)$$

$$\hat{C} [\cosh(\hat{\Psi}_S) - \cosh(\hat{\Psi}_b)] = \hat{\Gamma}_S^2. \quad (A4)$$

Here  $\hat{y} = y/b$  is a dimensionless distance,  $\hat{C}$  is a dimensionless concentration, and  $\hat{\Gamma}_S$  is a dimensionless surface charge density. The latter are defined by

$$\hat{C} = \frac{16 \pi N_A^2 e^2 b^2 C}{D R T} \quad (A5)$$

$$\hat{\Gamma}_S = \frac{4 \pi N_A e b \Gamma_S}{D R T}. \quad (A6)$$

When  $\hat{C}$  and  $\hat{\Gamma}_S$  are specified, (A3) and (A4) can be solved to obtain  $\hat{\Psi}$  as a function of distance from the clay surfaces.  $\hat{\Psi}_S$  and  $\hat{\Psi}_b$  are not known a priori, but must be computed from (A3) and (A4) iteratively [e.g., *Bresler*, 1970]. Thus  $\hat{\Psi} = \hat{\Psi}(\hat{C}, \hat{\Gamma}_S)$ , that is,  $\hat{\Psi}$  depends only on  $\hat{C}$  and  $\hat{\Gamma}_S$ .

[55] Once  $\hat{\Psi}$  has been determined, the anion concentration anywhere in the pore space between the clay surfaces,  $C'$ , can be calculated from Boltzmann's equation, which is written as [Bresler, 1970]

$$\frac{C'}{C} = \exp(\hat{\Psi}). \quad (\text{A7})$$

Equation (A7) again assumes a monovalent ( $\nu = 1$ ) solute and expresses anion concentrations as moles per volume.  $C'$ , which through  $\hat{\Psi}$  is a function of distance  $y$  from the clay surface, is key to calculating osmotic efficiency  $\sigma$ .

[56] *Kemper and Evans* [1963] developed a pore-scale conceptual model for osmosis in clays, and *Kemper and Rollins* [1966] and *Boersma et al.* [1972] extended it to obtain a model for osmotic efficiency. *Bresler's* [1973] osmotic efficiency model is essentially a refinement of theirs. In brief, osmotic flows are viewed as the result of collisions between water molecules, solute molecules, and the porous medium. At the entrance to a pore throat, some ions transfer momentum from their random motion to the clay via repulsion by its electric potential field. That momentum is lost to the fluid, reducing the amount available to drive water molecules into and through the pore throat. The resulting force imbalance causes a net movement of water molecules in the direction of higher concentration where relatively more collisional momentum is absorbed by the clay. This is interpreted as the driving force represented by  $\nabla\pi$  (see equation (1)).

[57] A consequence of the molecular collision model is that within the pore throat, the actual driving force imposed by a macroscopic gradient in  $\pi$  varies with distance from the clay surface. This is because the vigor of ion exclusion and the fraction of collisional momentum absorbed by the clay varies with distance from the clay surface. Going a step further, *Kemper and Rollins* [1966] assumed that the force imbalance or osmotic driving force within a pore throat is proportional to the ion exclusion. Under this assumption the osmotic driving force parallel to the clay platelets (the  $x$  coordinate direction) can be written as

$$F_o = [1 - C'/C] \frac{d\pi}{dx}, \quad (\text{A8})$$

where  $1 - C'/C$  is called the salt exclusion factor.  $F_o$  varies with distance  $y$  from the clay surface via the dependence of  $C'$  on  $\hat{\Psi}$ . In large pores where  $C' = C$  except near the solid surfaces, (A8) shows that  $F_o = 0$  except near the solid surfaces, as expected. On the other hand, when all solute is excluded and  $C' = 0$  for all  $y$ ,  $F_o$  takes its maximum value of  $d\pi/dx$  for all  $y$ .

[58] Flow between parallel plates, such as clay platelets, is also affected by viscous drag, causing the velocity to vary with distance from the plates. Between plates located at  $y = 0$  and  $y = 2b$  the velocity is [e.g., *Lamb*, 1945]

$$u = \frac{1}{2\mu} (2by - y^2) F, \quad (\text{A9})$$

where  $\mu$  is the fluid's dynamic viscosity [ $\text{ML}^{-1} \text{T}^{-1}$ ] and  $F$  is the overall driving force [ $\text{ML}^{-2} \text{T}^{-2}$ ].

[59] *Kemper and Rollins* [1966] then substituted (A8) into (A9) under the assumption that  $F$  can be equated with  $F_o$ , arriving at

$$u = \frac{1}{2\mu} (2by - y^2) [1 - C'/C] \frac{d\pi}{dx} \quad (\text{A10})$$

as a description of the velocity of osmotically driven flow between parallel clay platelets comprising a pore throat. The validity of equating  $F_o$  and  $F$  is dubious, as we discuss in section A2. For the moment, however, we simply accept this step in the development.

[60] The osmotic efficiency  $\sigma$  of a membrane can be considered to be the ratio of the osmotic flux it can generate to that generated by a perfect membrane. Thus, following the conceptual model of *Kemper and Rollins* [1966] outlined above, *Bresler* [1973] concluded that osmotic efficiency can be calculated as

$$\sigma = \frac{\int_0^b [2by - y^2] [1 - C'/C] dy}{\int_0^b [2by - y^2] dy}, \quad (\text{A11})$$

where the integrals in the numerator and denominator represent the average osmotic flow velocities in the nonperfect and equivalent perfect membrane, respectively. The latter is obtained simply by setting  $C' = 0$  for all  $y$ . *Kemper and Rollins* [1966] presented an expression analogous to (A11) expressed as discrete sums rather than integrals.

[61] Substituting (A7) into (A11) and writing the latter in terms of  $\hat{y}$  yields a fully nondimensional form, namely,

$$\sigma = \frac{\int_0^1 [2\hat{y} - \hat{y}^2] [1 - \exp(\hat{\Psi})] d\hat{y}}{\int_0^1 [2\hat{y} - \hat{y}^2] d\hat{y}}. \quad (\text{A12})$$

Equations (A12) and (A7) imply that  $\sigma$ , like  $\hat{\Psi}$ , depends only on  $\hat{C}$  and  $\hat{\Gamma}_S$ . That is,  $\sigma = \sigma(\hat{C}, \hat{\Gamma}_S)$ . Referring to (A5) and (A6), which define these quantities, we note that  $N_A$ ,  $e$ , and  $R$  are constants. Thus

$$\sigma = \sigma\left(\frac{b^2 C}{DT}, \frac{b\Gamma_S}{DT}\right). \quad (\text{A13})$$

*Bresler* [1973] found that  $\sigma$  is insensitive to  $\Gamma_S$ , with order-of-magnitude changes in the latter causing  $\sigma$  to differ by about 10%. Thus

$$\sigma \approx \sigma\left(\frac{b^2 C}{DT}\right) \approx \sigma\left(\frac{b\sqrt{C}}{\sqrt{DT}}\right). \quad (\text{A14})$$

Moreover, the square root of  $DT$ , the product of relative permittivity of the pore water and absolute temperature, varies by less than a factor of approximately 1.3. Thus

$$\sigma \approx \sigma(b\sqrt{C}). \quad (\text{A15})$$

Because of this property of the *Kemper and Rollins* [1966] model, *Bresler* [1973] was able to approximate behavior in different clay media using a single curve relating  $\sigma$  to  $b\sqrt{C}$  as in our Figure 2.

### A1. Error in Predicted $\sigma$ and $p_o$

[62] As just noted, errors in  $\sigma$  of approximately 10% result from ignoring its functional dependence on the second term in (A13), with additional error resulting from ignoring the dependence of  $\sigma$  on  $D$  through the first term in (A13). In addition, we suspect some error in  $\sigma$  results from flaws in *Kemper and Rollins's* [1966] conceptual model of osmotic flow, which are described in section A2. On the basis of differences between predicted and observed behavior in modified clays shown by *Bresler* [1973, Figure 1], we estimate the total error in predicted  $\sigma$  can be as great as a factor of  $\sim 3$ . However, errors in  $\sigma$  are significantly less in our analysis because we fit observed  $\sigma$  values to *Bresler's* curve. This is equivalent to translating data along the  $b\sqrt{C}$  axis by adjusting  $b$ . This yields effective rather than actual values of the physical properties that  $b$  and  $A_{so}$  represent, and these effective values incorporate most of the error. When  $A_{so}$  values are then used to predict osmotic pressure  $p_o$  for the same medium under a different concentration regime by reversing the computations, the same errors are essentially subtracted out. The remaining error in predicted  $\sigma$  is difficult to determine, but based on scatter in the few available data, we estimate that it is a factor of  $\sim 1.5$  or less for  $\sigma > 0.1$ , the range most affecting our predictions of  $p_o$ . The same error estimates apply to predicted values of  $p_o$ .

### A2. Critique of the Bresler Model

[63] Certain aspects of *Bresler's* [1973] osmotic efficiency model might be expected to limit its utility. These include an apparent conceptual inconsistency in its development and the highly idealized nature of clay membranes that it posits.

[64] We alluded above to a theoretical difficulty underlying (A10), an equation developed to describe pore-scale velocity distributions in osmotically driven flows. The equation was derived by *Kemper and Rollins* [1966], discussed further by *Boersma et al.* [1972], and adopted by *Bresler* [1973] as the basis of his osmotic efficiency model. The difficulty arises from (A8), which describes osmotic driving force  $F_o$  in pore throats.  $F_o$  varies with distance  $y$  from the clay surface because of its dependence on the nondimensional electrical potential  $\hat{\Psi}$ . *Kemper and Rollins* [1966] and *Boersma et al.* [1972] substituted  $F_o$  into (A9), an expression for velocity in a fluid flowing between parallel plates that is well known from classical hydrodynamics [e.g., *Lamb*, 1945]. The substitution assumes that  $F_o$  can be equated with hydraulic driving force  $F$  in (A9). However, a premise of the derivation of (A9) is that  $F$  is constant across the aperture [*Lamb*, 1945, p. 582]; substitution of  $F_o$  for  $F$  violates this premise. Indeed, the velocity distribution described by (A9) is due to fluid drag on the bounding walls and viscous shear in the fluid. In contrast, the *Kemper and Rollins* model hypothesizes that velocity variation across pore throats is due to variation in the driving force, making (A10) internally inconsistent.

[65] *Kemper and Rollins* [1966] and *Boersma et al.* [1972] also assume a highly idealized clay medium. Their analysis considers pore throats to be bounded by parallel clay platelets. Moreover, their use of a one-dimensional analysis tacitly assumes that the aperture between the platelets is small compared with the extent of the clay surfaces. While microstructural models that invoke elongated pore throats are able to explain certain macroscopic petrophysical properties of shales [*Katsube and Williamson*, 1998], it is unlikely that they are formed by parallel clay platelets. In addition, the *Kemper and Rollins* model considers pore throats of a single size whereas both pore and pore throat sizes in clay media are not uniform and are usually described using a probability distribution [e.g., *Katsube and Williamson*, 1998].

### A3. Calculating $A_{so}$ From Osmosis Test Data

[66] Solutions of (A11) or (A12) for a range of values of clay surface charge density  $\Gamma_S$  yield a family of curves in  $\sigma$  versus  $b\sqrt{C}$  space. *Bresler* [1973] apparently chose the curve that gave the best fit to available data, obtaining his Figure 1, a plot similar to our Figure 2a. To avoid introducing bias, and because *Bresler's*  $\sigma$  versus  $b\sqrt{C}$  curve seems to describe both processed and unmodified geologic media well, we simply adopted it to specify  $\sigma(C)$  in (7). Because *Bresler* fitted the curve visually, it was represented using a graphical approximation. Thus an expression for  $b$  cannot be derived from (7).

[67] Values of  $p_o$  were calculated by solving (7) numerically. Spline functions were fitted to a table of  $\sigma$  and  $b\sqrt{C}$  values obtained graphically from *Bresler's* curve and to a table of  $\pi$  and  $C$  values, with the latter calculated from a tabulation of  $a_w$  versus  $C$  for NaCl [*Robinson and Stokes*, 2002] after converting  $C$  from moles per unit volume to moles per unit mass. Splines were fitted using the Akima algorithm implemented through the International Mathematical and Statistics Libraries, Inc. (IMSL) routine CSAKM,  $d\pi/dC$  was evaluated using the IMSL routine CSDER, and integration was done using the IMSL routine QDAG [*Visual Numerics*, Inc., 1998].

### References

- Al-Bazali, T. M. (2005), Experimental study of the membrane behavior of shale during interaction with water-based and oil-based muds, Ph.D. thesis, 272 pp., Univ of Tex. at Austin. (Available at <http://www.pge.utexas.edu/theses05/talal.pdf>)
- Bekele, E. B., M. A. Person, B. J. Rostron, and R. Barnes (2002), Modeling secondary oil migration with core-scale data: Viking Formation, Alberta Basin, *AAPG Bull.*, 86(1), 55–74.
- Boersma, L., et al. (1972), Isothermal flow of nonhomogeneous aqueous solutions, in *Soil Water*, chap. 6, pp. 121–154, edited by D. R. Nielson et al., Soil Sci. Soc. of Am., Madison, Wisc.
- Boisson, J.-Y. (2005), Clay Club catalogue of characteristics of argillaceous rocks, *Nucl. Energy Agency Rep. 4436*, 217 pp., Organ. for Econ. Coop. and Dev., Issy-les-Moulineaux, France.
- Bradley, J. S. (1975), Abnormal formation pressure, *AAPG Bull.*, 59(6), 957–973.
- Bredehoeft, J. D., J. B. Wesley, and T. D. Fouch (1994), Simulations of the origin of fluid pressure, fracture generation, and the movement of fluids in the Uinta Basin, Utah, *AAPG Bull.*, 78(11), 1729–1747.
- Bresler, E. (1970), Numerical solution of the equation for interacting diffuse layers in mixed ionic systems with nonsymmetrical electrolytes, *J. Colloid Interface Sci.*, 33(2), 278–283.
- Bresler, E. (1973), Anion exclusion and coupling effects in nonsteady transport through unsaturated soils: I. Theory, *Soil Sci. Soc. Am. Proc.*, 37(5), 663–669.

- Cey, B. D., S. L. Barbour, and M. J. Hendry (2001), Osmotic flow through a Cretaceous clay in southern Saskatchewan, Canada, *Can. Geotech. J.*, 38(5), 1025–1033, doi:10.1139/cgj-38-5-1025.
- Domenico, P. A., and F. W. Schwartz (1990), *Physical and Chemical Hydrogeology*, 824 pp., John Wiley, New York.
- Fritz, S. J. (1986), Ideality of clay membranes in osmotic processes: A review, *Clays Clay Miner.*, 34(2), 214–223, doi:10.1346/CCMN.1986.0340212.
- Fritz, S. J., and I. W. Marine (1983), Experimental support for a predictive osmotic model of clay membranes, *Geochim. Cosmochim. Acta*, 47(8), 1515–1522, doi:10.1016/0016-7037(83)90310-1.
- Fritz, S. J., and T. M. Whitworth (1994), Hyperfiltration-induced fractionation of lithium isotopes: Ramifications relating to representativeness of aquifer sampling, *Water Resour. Res.*, 30(2), 225–235, doi:10.1029/93WR02682.
- Garavito, A. M., H. Kooi, and C. E. Neuzil (2006), Numerical modeling of a long-term in situ chemical osmosis experiment in the Pierre Shale, South Dakota, *Adv. Water Resour.*, 29(3), 481–492, doi:10.1016/j.advwatres.2005.06.004.
- Garavito, A. M., P. De Cannière, and H. Kooi (2007), In situ chemical osmosis experiment in the Boom Clay at the Mol underground research laboratory, *Phys. Chem. Earth*, 32(1–7), 421–433.
- Gonçalvès, J., S. Violette, and J. Wendling (2004), Analytical and numerical solutions for alternative overpressuring processes: Application to the Callovo-Oxfordian sedimentary sequence in the Paris basin, France, *J. Geophys. Res.*, 109, B02110, doi:10.1029/2002JB002278.
- Greenberg, J. A., J. K. Mitchell, and P. A. Witherspoon (1973), Coupled salt and water flows in a groundwater basin, *J. Geophys. Res.*, 78(27), 6341–6353, doi:10.1029/JC078i027p06341.
- Gretener, P. E. (1981), Abnormal pore fluid pressures: Definition, terminology, observations, in *Pore Pressure Fundamentals, General Ramifications, and Implications for Structural Geology Educ. Course Not. Ser.*, vol. 4, pp. 34–43, Am. Assoc. of Pet. Geol., Tulsa, Okla.
- Groenevelt, P. H., and G. H. Bolt (1969), Non-equilibrium thermodynamics of the soil-water system, *J. Hydrol.*, 7(4), 358–388, doi:10.1016/0022-1694(69)90092-4.
- Gueutin, P., S. Altmann, J. Gonçalvès, P. Cosenza, and S. Violette (2007), Osmotic interpretation of overpressures from monovalent based triple layer model, in the Callovo-Oxfordian at the Bure site, *Phys. Chem. Earth*, 32(1–7), 434–440.
- Hendry, M. J., and F. W. Schwartz (1988), An alternative view on the origin of chemical and isotopic patterns in groundwater from the Milk River Aquifer, Canada, *Water Resour. Res.*, 24(10), 1747–1763, doi:10.1029/WR024i010p01747.
- Katsube, T. J., and M. A. Williamson (1998), Shale petrophysical characteristics: Permeability history of subsiding shales, in *Shales and Mudstones*, edited by J. Schieber, W. Zimmerle, and P. S. Sethi, pp. 69–91, Schweizerbart, Stuttgart, Germany.
- Keijzer, T. J. S. (2000), Chemical osmosis in natural clayey materials, Ph.D. thesis, 166 pp., Univ. of Utrecht, Utrecht, Netherlands.
- Kemper, W. D. (1961), Movement of water as effected by free energy and pressure gradients: II. Experimental analysis of porous systems in which free energy and pressure gradients act in opposite directions, *Soil Sci. Soc. Am. Proc.*, 25(4), 260–265.
- Kemper, W. D., and N. A. Evans (1963), Movement of water as effected by free energy and pressure gradients: III. Restriction of solutes by membranes, *Soil Sci. Soc. Am. Proc.*, 27(5), 485–490.
- Kemper, W. D., and J. P. Quirk (1972), Ion mobilities and electric charge of external clay surfaces inferred from potential differences and osmotic flow, *Soil Sci. Soc. Am. Proc.*, 36(3), 426–433.
- Kemper, W. D., and J. B. Rollins (1966), Osmotic efficiency coefficients across compacted clays, *Soil Sci. Soc. Am. Proc.*, 30(5), 529–534.
- Lamb, H. (1945), *Hydrodynamics*, 738 pp., Dover, Mineola, N. Y.
- Lee, Y., and D. Deming (2002), Overpressures in the Anadarko basin, southwestern Oklahoma: Static or Dynamic?, *AAPG Bull.*, 86(1), 145–160.
- Letey, J., W. D. Kemper, and L. Noonan (1969), The effect of osmotic pressure gradients on water movement in unsaturated soil, *Soil Sci. Soc. Am. Proc.*, 33(1), 15–18.
- Malusis, M. A., and C. D. Shackelford (2004), Predicting solute flux through a clay membrane barrier, *J. Geotech. Geoenviron. Eng.*, 130(5), 477–487, doi:10.1061/(ASCE)1090-0241(2004)130:5(477).
- Marine, I. W. (1974), Geohydrology of buried Triassic basin at Savannah River Plant, South Carolina, *Am. Assoc. Pet. Geol. Bull.*, 58(9), 1825–1837.
- Marine, I. W., and S. J. Fritz (1981), Osmotic model to explain anomalous hydraulic heads, *Water Resour. Res.*, 17(1), 73–82, doi:10.1029/WR017i001p00073.
- Mitchell, J. K. (1993), *Fundamentals of Soil Behavior*, 437 pp., John Wiley, New York.
- Neuzil, C. E. (1994), How permeable are clays and shales?, *Water Resour. Res.*, 30(2), 145–150, doi:10.1029/93WR02930.
- Neuzil, C. E. (2000), Osmotic generation of “anomalous” fluid pressures in geological environments, *Nature*, 403(6766), 182–184, doi:10.1038/35003174.
- Noy, D. J., S. T. Horseman, J. F. Harrington, P. Bossart, and H. R. Fisch (2004), An experimental and modelling study of chemico-osmotic effects in the Opalinus Clay of Switzerland, in *Mont Terri Project—Hydrogeological Synthesis, Osmotic Flow, Geol. Ser.*, vol. 6, edited by P. Heitzman, pp. 95–126, Fed. Off. for Water and Geol., Bern, Switzerland.
- Olsen, H. W. (1962), Hydraulic flow through saturated clays, *Clays Clay Miner.*, 9, 131–161, doi:10.1346/CCMN.1960.0090108.
- Olsen, H. W. (1969), Simultaneous fluxes of liquid and charge in saturated kaolinite, *Soil Sci. Soc. Am. Proc.*, 33(3), 338–344.
- Osborne, M. J., and R. E. Swarbrick (1997), Mechanisms for generating overpressure in sedimentary basins: A reevaluation, *AAPG Bull.*, 81(6), 1023–1041.
- Patchett, J. G. (1975), An investigation of shale conductivity, *Trans. SPWLA Annu. Logging Symp.*, 16, 41 pp.
- Rahman, M. M., Z. Chen, and S. S. Rahman (2005), Experimental investigation of shale membrane behavior under tri-axial condition, *Pet. Sci. Technol.*, 23(9–10), 1265–1282, doi:10.1081/LFT-200035734.
- Robinson, R. A., and R. H. Stokes (2002), *Electrolyte Solutions*, 2nd ed., 571 pp., Dover, Mineola, N. Y.
- Schultz, L. G., H. A. Tourtelot, J. R. Gill, and J. G. Boerngen (1980), Composition and properties of the Pierre Shale and equivalent rocks, northern Great Plains region, U.S. Geol. Surv. Prof. Pap., 1064-B, 114 pp.
- Spencer, C. W. (1994), Abnormal formation pressures caused by hydrocarbon generation: Examples from the Rocky Mountain Region, in *Studies in Abnormal Pressures, Dev. Pet. Sci.*, vol. 38, edited by W. H. Fertl, R. E. Chapman, and R. F. Hotz, chap. 12, pp. 343–375, Elsevier, Amsterdam.
- van Oort, E. (1994), A novel technique for the investigation of drilling fluid induced borehole instability in shales, in *Proceedings of Eurock '94 SPE/ISRM International Conference*, pp. 293–308, A. A. Balkema, Rotterdam, Netherlands.
- van Oort, E., A. H. Hale, and F. K. Mody (1995), Manipulation of coupled osmotic flows for stabilisation of shales exposed to water-based drilling fluids, SPE paper 30499 presented at the SPE Annual Technical Meeting and Exhibition, Dallas, Tex., 22–25 Oct.
- van Ruth, P., R. Hillis, P. Tingate, and R. Swarbrick (2003), The origin of overpressure in “old” sedimentary basins: An example from the Cooper Basin, Australia, *Geofluids*, 3(2), 125–131, doi:10.1046/j.1468-8123.2003.00055.x.
- Visual Numerics, Inc. (1998), *IMSL Fortran 90 MP Library User's Guide*, Houston, Tex.
- Young, A., and P. F. Low (1965), Osmosis in argillaceous rocks, *Bull. Am. Assoc. Pet. Geol.*, 49(7), 1004–1007.

C. E. Neuzil and A. M. Provost, U.S. Geological Survey, 431 National Center, Reston, VA 20192, USA. (ceneuzil@usgs.gov; aprovest@usgs.gov)